THE JOURNAL OF PHYSICAL CHEMISTRY LETTERS
A JOURNAL OF THE AMERICAN CHEMICAL SOCIETY

pubs.acs.org/JPCL Letter

Directly Measuring the Connectivity between Isoenergetic Light-Harvesting Antennas in Plant Photosystem II at Physiological Temperature

Hoang Long Nguyen, Kai Zhong, Thanh Nhut Do, Parveen Akhtar, Petar H. Lambrev, Thomas L. C. Jansen, Jasper Knoester, Stefano Caffarri, and Howe-Siang Tan*

Cite This: https://doi.org/10.1021/acs.jpclett.5c02240 Read Online

ACCESS | Metrics & More | Article Recommendations | Supporting Information

ABSTRACT: The plant photosystem II (PSII) supercomplex features a relatively "flat" energy landscape in the excitonic energy transfer (EET) network between the light-harvesting antenna and core subunits. The resulting intersubunit EET proceeds predominantly between isoenergetic excitonic states. Visualizing these EET dynamics is difficult due to the heavy spectral overlaps between the components, particularly at physiological temperature. We employ polarization-resolved two-dimensional electronic spectroscopy to measure and compare the anisotropy kinetics between the LHCII-CP29-CP24 complex and some of its constituents. Using the orientational differences between the subunits, together with the EET time scales estimated from energy transfer theory and phenomenological kinetic modeling, we identify the contribution of intra- and intersubunit EET processes to the observed anisotropy decay components. The results suggest that EET rates between the antenna subunits are not homogeneous and can be sensitive to the interprotein arrangement. The approach provides an effective method for studying EET in large multichromophoric systems.

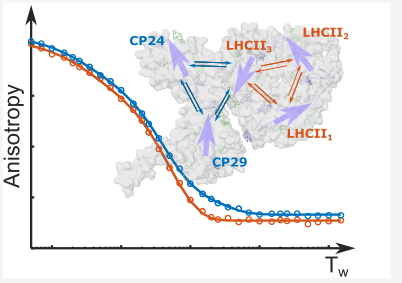

In higher plants, the photosynthesis process starts with the chromophore−protein light-harvesting complexes (LHCs), typically organized into coordinated groups known as photosystems.[1] The plant photosystem II (PSII) consists of the reaction centers (RCs) embedded in the core complexes, and several subunits of peripheral antenna LHCs.[2,3] PSII relies on excitonic energy transfer (EET) to distribute the absorbed light energy, which can occur at the intrasubunit (within an individual subunit) and intersubunit levels (between the subunits). Intrasubunit EET processes, especially in the light-harvesting complex II (LHCII), have been extensively investigated with spectroscopic and theoretical means.[4−14] Regarding the dynamics in the PSII supercomplex, there have also been studies focusing on the collective exciton dynamics, revealing a general idea about the diffusion speed of excitation across the photosystem.[2,15,16] Advances in purification procedures of small subgroups of the supercomplex[17] have enabled selective studies of interactions between a few PSII subunits while avoiding the contributions from other components that could complicate the spectra.[18−21] However, intersubunit EET processes are mostly observed at cryogenic temperature, while in physiological conditions they are largely obscured by the significant overlaps between the subunit spectral features. In addition, the spectroscopic similarities between the subunits also imply a lack of clear directionality in the EET channels to the RCs, which is hypothetically a feature to help PSII adapt and maintain its robustness from environmental fluctuations by accommodating multiple EET pathways.[1,22−24] Understanding the mechanisms and pathways of physiological EET processes, therefore, provides insights into the optimization strategies and functional roles of PSII and its constituents, ultimately revealing the design principles employed in natural photosynthesis.

Two-dimensional electronic spectroscopy (2DES) is a nonlinear optical spectroscopic technique capable of resolving complex dynamical processes with femtoseconds (fs) to picoseconds (ps) time scales. A 2DES spectrum correlates the excitation with detection frequencies, and through the diagonal and cross-peaks therein, it presents the EET between the excitonic states of the system.[25,26] In 2DES, polarization control makes use of the relative polarizations of the pump and probe laser fields to manipulate the intensities of signals through the orientations of the transition dipoles.[27] The scaling of signal intensities with the pump−probe polarization allows the user to separately control the signal contributions to the 2DES spectra and increase the visibility of specific spectral features, such as cross-peaks,[28−33] beating patterns,[34,35] and orientational dynamics (polarization anisotropy).[36,37] Polar-

Received: July 21, 2025
Revised: December 4, 2025
Accepted: December 12, 2025

ization anisotropy information is usually overlooked in 2DES measurement, as isotropic 2D signals are often preferred and easily collected with magic angle pump−probe polarization. However, given that the EET processes between molecules can be associated with changes in transition dipole orientations, anisotropy can be a potentially useful indicator for dynamical processes involving isoenergetic states.

In this article, we report on the observation of intersubunit isoenergetic EET processes in a subgroup of antenna LHCs in PSII. The difficulty of resolving EET between isoenergetic states is overcome by leveraging on the polarization dependence of signals from the chromophores in the LHCs. Specifically, we perform 2DES with polarization control to obtain 2D maps containing anisotropic information, which we term the 2D relaxation of electronic anisotropy maps (2DREAM). Here, we measure the 2DREAM of the trimeric light-harvesting complex II (LHCII), monomeric LHCII, and LHCII(M)-CP29-CP24 (also termed M-CP_2, the complex containing a moderately bound LHCII and the minor antennas CP29 and CP24 in PSII). Our study is conducted at room temperature to ensure the dynamical processes happening at near physiological conditions. Previous measurements of the anisotropy dynamics in LHCII were mostly done in the nineties, which agreed upon a 5 ps anisotropy lifetime in the complex at room temperature.[37−40] Measurement at various pairs of excitation/detection wavelengths also observed different residual anisotropy values and slight deviations of the anisotropy decay lifetime.[38] Utilizing the advantages of 2DES, we demonstrate that the use of 2DREAM can provide frequency-resolved anisotropy kinetics with high time resolution. By comparing the anisotropy kinetics between M-CP_2 and the smaller antenna complexes, we gain insights into the EET between the LHC subunits. We also employ theoretical tools and phenomenological kinetic modeling to support the experimental observations.

M-CP_2 is located at the periphery of the PSII-LHCII supercomplex structure, connecting to the RC via the core-integrated antenna CP47. In Figure 1a, we highlight the position of the M-CP_2 subunits in the cryo-EM structure of the $C_2S_2M_2$-type PSII-LHCII supercomplex (PDB 5XNM).[41] In total, 66 Chl molecules can be found in M-CP_2, including 39 Chls *a* and 27 Chls *b*. The absorption spectrum of M-CP_2 at room temperature is presented in Figure 1b, in comparison with the trimeric and monomeric LHCIIs. In the spectra, the Q_y absorption bands of Chl *a* and Chl *b* can be found at 675 and 650 nm, respectively. The absorbing region spanning from 300 to 500 nm contains features from carotenoids and the Chl Soret bands. By normalizing at the Chl *a* Q_y absorption peak (at 675 nm), M-CP_2 exhibits less absorbance at 650 nm due to its lower Chl *b* concentration. The Q-band absorption in LHCII trimers and monomers are nearly identical. M-CP_2 also shows a lower absorption in the 300−500 nm region due to a lower concentration of carotenoids relative to the other complexes.[3] Throughout this study, we focus on the Chl Q_y region and apply a pump spectrum from 600 to 700 nm in the 2DES experiments (shaded area in Figure 1b).

We conducted polarization-resolved 2DES measurements at room temperature on M-CP_2, LHCII trimers, and LHCII monomers. Here, we only present the results for M-CP_2, while the spectra of LHCII trimers and monomers can be found in the Supporting Information (SI). For the minor antenna complexes CP24 and CP29 contained in M-CP_2, their individual kinetics are not readily available but assumed to

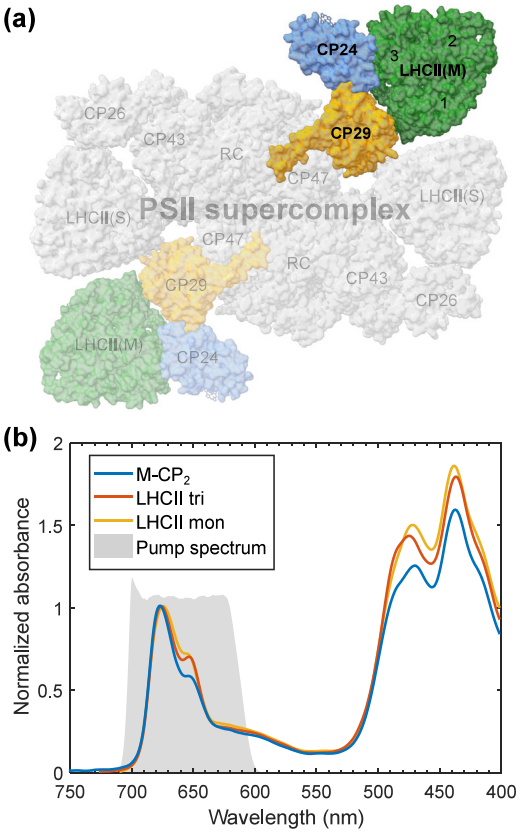

Figure 1. (a) The apoprotein surface of the $C_2S_2M_2$-type PSII-LHCII supercomplex, in which the subunits of M-CP_2 are highlighted in colors. The monomeric subunits in LHCII(M) are numbered 1−3. Since PSII is a homodimer, M-CP_2 occurs in both halves. (b) Linear absorption spectra of M-CP_2 (blue), LHCII trimers (red), and LHCII monomers (yellow), normalized at the Chl *a* Q_y peak. The pump spectrum used in 2DES experiments is also shown as a gray-shaded area.

be similar to those in monomeric LHCII. This assumption is made based on the similar protein structures and chromophore compositions between the antenna complexes.[3] In addition, data on steady state and pump−probe spectroscopy of the minor antennas at room temperature suggests large resemblance to those of LHCII to a large extent, especially at the Chl *a* absorption region.[6,21,42]

Parallel- and perpendicular-polarized 2D spectra are collected simultaneously from the same measurement, which can be combined post-measurement to reconstruct 2D spectra with different pump−probe polarization conditions (see Experimental methods in SI). In Figure 2a, we present the 2DREAM, i.e., the reconstructed 2D maps measuring polarization anisotropy. Each anisotropy value at λ_τ/λ_t on the 2DREAM reflects the angular alignment between the transition dipoles of the excited state λ_τ and the detected state λ_t. Generally, the time-resolved dynamics on the 2DREAM represent the time-resolved anisotropy at every pair of excitation and detection wavelengths, which evolve due to rotational motions and EET processes. In the areas with spectral overlaps between multiple exciton states, the measured anisotropy kinetics can be a weighted combination of multiple EET processes, depending on the EET amplitudes and the resulting changes in exciton dipole orientations (see SI).

https://doi.org/10.1021/acs.jpclett.5c02240
J. Phys. Chem. Lett. XXXX, XXX, XXX−XXX

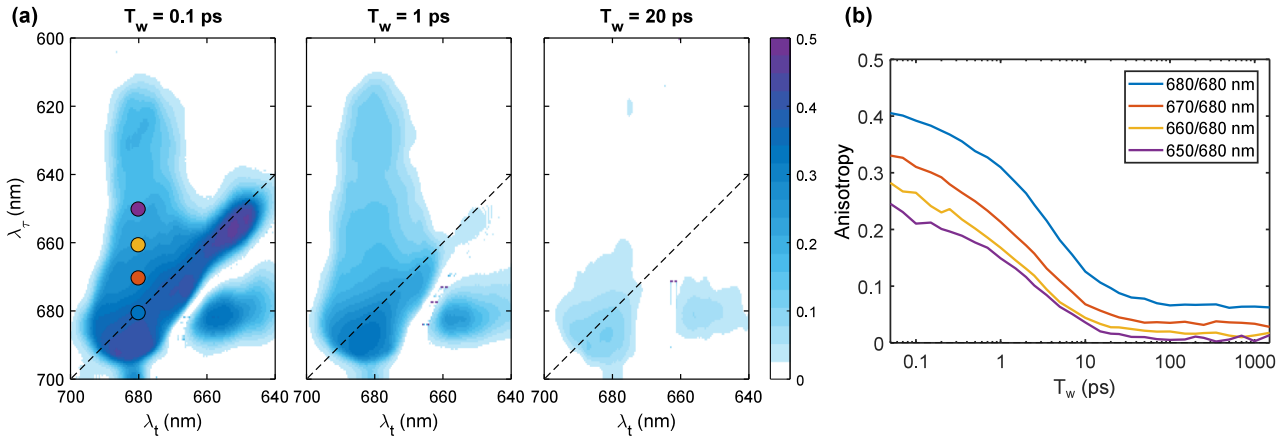

Figure 2. 2D relaxation of electronic anisotropy maps (2DREAM) of M-CP_2, reconstructed from 2D spectra measured at parallel and perpendicular pump−probe polarization. (a) 2DREAM at waiting times 0.1, 1, and 20 ps are shown. All spectra use the same color scale. (b) Anisotropy kinetics from T_w = 50 fs to 1.5 ns at several peaks detected at 680 nm, as marked on the 2D spectrum at 0.1 ps. Here, the pixels with low signal-to-noise ratio are set at zero. The anisotropy values are also limited between 0 and 0.5.

From Figure 2a, most anisotropies along the diagonal line are close to 0.4 at T_w = 0.1 ps. Meanwhile, the anisotropy around the 650 nm diagonal peak reaches nearly 0.5, probably influenced by excited-state absorption signals from the lower-energy excited states.[43,44] Anisotropy values for the cross-peaks are generally lower, even at the shortest T_w. To be specific, at the detection wavelength of λ_t = 680 nm, the anisotropy value at T_w = 0.1 ps from long to short excitation wavelengths gradually decreases from 0.4 (λ_τ = 680 nm) to 0.2 (λ_τ = 620−640 nm). The reason is that anisotropy value reflects the relative orientation between the excited and detected transitions. Since on a diagonal signal at early waiting time, the excitation and detection largely come from the same transition, the anisotropy value here should be higher than those on the cross-peaks, where the excitation and detection are likely made on different exciton states. By T_w = 1 and 20 ps, EET dynamics have caused depolarization among the underlying excitons, as observed by the smaller anisotropy values in the 2DREAM at these delay times. Figure 2b shows the anisotropy decay curves of the 680 nm diagonal and several cross-peaks. Generally, the anisotropy kinetic traces exhibit decaying trends due to depolarization among the underlying energy levels, occurring across multiple time scales from sub-ps to several ps. The decays equilibrate soon after T_w = 100 ps. Around the terminal state diagonal peak, 680/680 nm, the residual anisotropy, i.e., equilibrated anisotropy value at late T_w, is at around 0.06. Comparing between different excitation wavelengths, the residual anisotropies are smaller at cross-peaks with shorter λ_τ. The anisotropy kinetics remain almost flat after T_w = 100 ps, which reflects their independence of spontaneous relaxation processes.

Comparing to published literature measuring the anisotropy in trimeric LHCII, we found that Kwa et al. measured one-color pump−probe at several diagonal positions from 645 to 685 nm. The residual anisotropies varied between −0.05 and 0.05, especially at the long wavelengths, 0.00 ± 0.03 at 675 nm and 0.02 ± 0.03 at 670 nm.[38] Similar measurements by Savikhin et al. reported residual values reducing from 0.05 at 685 nm to 0.00 at 670 nm.[40] These results are similar to the residual values of the 2DREAM around the 670−680 nm spectral region, which show values varying from around 0.06 at the 680 nm diagonal peak to around 0.03 at 670/680 nm. Due to the slow instrumental responses intrinsic to the techniques in those studies, we found discrepancies to our results at the early, sub-ps delay times. For example, the initial anisotropies were found to be 0.32−0.34 by Savikhin et al.,[40] whereas our measured values are close to 0.4, with a better time resolution of around 50 fs in our 2DES setup. Furthermore, the anisotropy decay lifetimes were reported to be 5 ps at all wavelengths in most studies. Meanwhile, a sub-ps decay component can be observed in our 2DES spectra (Figure 2b), which was also reported in an earlier fluorescence upconversion study featuring around 100 fs time resolution.[39]

To focus on the energy equilibration process between the terminal energy levels, we make a comparison of anisotropy kinetics at around 680 nm, contrasting between M-CP_2, LHCII trimers, and LHCII monomers. The time and frequency resolution of 2DREAM allow for wavelength-specific measurements while still capturing sub-100 fs anisotropy dynamics. In Figure 3, we plot the anisotropy decay curves of the three complexes, taken around the 680 nm diagonal peak in the 2DREAM. The anisotropy dynamics reflect energy transfer between exciton states around the terminal energy levels. The decay curves are averaged from multiple sets of independent

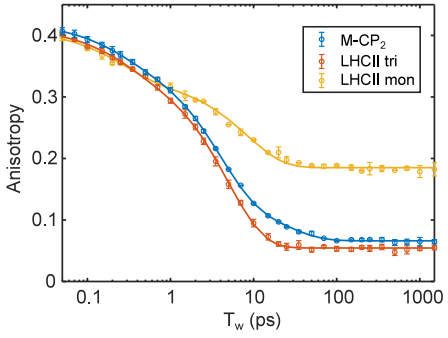

Figure 3. Comparison of the anisotropy decay kinetics observed at 680/680 nm on the 2DREAM, with 2 nm bandwidths, between M-CP_2 (blue circles), LHCII trimers (red circles), and LHCII monomers (yellow circles). The data points indicate the mean and standard deviation from independent measurements. Multiexponential fit results are plotted in solid curves.

https://doi.org/10.1021/acs.jpclett.5c02240
J. Phys. Chem. Lett. XXXX, XXX, XXX−XXX

measurements on different batches of samples (see Supporting Figure S3).

Overall, the anisotropies in all complexes start at around 0.4 at T_w = 50 fs, then decay together to 0.3 at T_w = 1 ps. After that, the decay curves start to diverge. In M-CP_2, the anisotropy decay continues until around T_w = 100 ps, where the residual value equilibrates at 0.06. In LHCII trimers, the decay reaches a residual value of 0.05 at an earlier T_w = 20 ps. The monomeric LHCII exhibits a weaker anisotropy decay, where the residual value is achieved at 0.19 after T_w = 20 ps. We highlight two key observations crucial to our subsequent discussion. First, the residual anisotropy of M-CP_2 is greater than that of trimeric LHCII. Second, a shoulder appears in the 10−100 ps range, indicating an additional decay component in M-CP_2 that is absent in the LHCII trimers. Both observations are statistically significant, as confirmed by the mean and standard deviations derived from multiple experimental runs.

Naively, one may expect that a larger ensemble of molecules should exhibit a more isotropic final distribution in chromophore orientations. This trend can be seen when moving from LHCII monomers to trimers. Since M-CP_2 is a larger group of protein complexes than LHCII, it may be expected to exhibit a smaller residual anisotropy. Instead, the residual anisotropy in M-CP_2 observed in Figure 3 is higher compared to LHCII trimers. This suggests a more aligned orientation distribution among the chromophores in the bigger complex. To explain this, we investigate the differences in Chl orientations between the subunits in the protein structure of M-CP_2.[41] Table 1 presents the relative rotation angles $\Delta\phi$ between the subunits in M-CP_2 around the normal axis of the complex. In the lower triangle, we indicate the cosine squares of these angles, which we call the alignment factors. An alignment factor close to one suggests a near parallelism between two corresponding subunits. In fact, the alignment factors suggest that CP29 and CP24 are aligned well with some of the LHCII monomers. On the other hand, since LHCII trimers have a 3-fold symmetry, the monomeric subunits are rotated 120° from each other, and their alignment factors are indeed around 0.25. Overall, the averaged alignment factor in M-CP_2 is 0.52, slightly higher than that in trimeric LHCII (0.5). Therefore, the inclusion of CP29 and CP24 makes the Chl arrangement in M-CP_2 less isotropic compared to that in LHCII trimers. In other words, this results in a higher likelihood for the excited state transitions in M-CP_2 to retain their original polarization during the energy equilibration process, and overall a slightly higher anisotropy value. This also highlights the sensitivity of anisotropy measurements in detecting structural differences among multichromophoric protein complexes.

Table 1. Alignment Factors between the Subunits in M-CP_2[a]

	$LHCII_1$	$LHCII_2$	$LHCII_3$	CP24	CP29
$LHCII_1$	-	120°	120°	111°	81°
$LHCII_2$	0.25	-	121°	18°	47°
$LHCII_3$	0.25	0.26	-	132°	155°
CP24	0.13	0.90	0.45	-	48°
CP29	0.03	0.46	0.82	0.45	-

[a]Lower triangle: The alignment factors, measured by the cosine squared of their relative rotation angles $\Delta\phi$ around the complex plane normal. Upper triangle: The angles $\Delta\phi$. Since the protein structures of the subunits are similar, $\Delta\phi$ can be found by determining the rotation matrix that transforms the set of Chl transition dipole vectors in one subunit to those in the other. The transition dipole is defined as the vector connecting the N_B and N_D atoms in the Chl chlorin ring. Here, for each pair of subunits, we only consider the common Chls that are present in both of them.

The anisotropy decay curves from 2DREAM in Figure 3 can be fitted with multiexponential decay functions to give the time scales of the underlying EET dynamics. The fit parameters are presented in Table 2. The anisotropy decay in LHCII trimers and monomers can be fitted with two lifetimes. Meanwhile, the decay in M-CP_2 cannot be accurately modeled with a biexponential decay function, but requires one additional long-lived component to be fully described. This additional component in M-CP_2 corresponds to the slowly decaying anisotropy segment observed at T_w = 10−100 ps. We confirm the choice between bi- and triexponential model based on cross-validating between independently measured data sets (see Supporting Figure S3 and S4). From Table 2, the first decay component in all complexes is resolved at similar sub-ps lifetimes of 0.23−0.26 ps. The amplitude of this fast decay process is relatively small, around 0.06−0.08 out of the initial anisotropy of 0.4. The second anisotropy decay component is fitted to a lifetime of 3.7 ps in M-CP_2, and contributes the most to the anisotropy decay with an amplitude of 0.23. In LHCII trimers, the process occurs at a slightly slower lifetime, 4.9 ps (amplitude 0.29). We note that this lifetime component has been observed in studies regarding anisotropy dynamics in LHCII.[37−40] LHCII monomers exhibit the slowest secondary decay among all complexes, with a lifetime of 8.3 ps and an amplitude of 0.14. A notable feature in the M-CP_2 anisotropy decay kinetics is the appearance of a slow depolarization process, happening at 24 ps. This 24 ps component therefore suggests a slow EET process that only occurs in M-CP_2 and not in the LHCII complexes.

Theoretical calculations can be used to aid the understanding of the EET drivers of the anisotropy decay processes. Here, we apply the recently developed time-domain multichromophoric fluorescence resonant energy transfer (TD-MCFRET) method.[45] We apply this approach to calculate the intersubunit EET times of the M-CP_2 complex. The structures of LHCII monomers, trimers, and M-CP_2 are extracted from the cryo-EM structure of PSII-LHCII supercomplex (PDB 5XNM).[41] The TD-MCFRET results can then be incorporated

Table 2. Fitted Parameters of the Multi-exponential Decay Fit, $f(T_w) = A_0 + \sum_i A_i \exp(-T_w/\tau_i)$, for the Anisotropy Decays in Figure 3[a]

Sample	A_1	τ_1	A_2	τ_2	A_3	τ_3	A_0
M-CP_2	0.055 (0.003)	0.23 (0.03)	0.23 (0.01)	3.7 (0.2)	0.069 (0.007)	24 (3)	0.066 (0.001)
LHCII tri.	0.064 (0.004)	0.26 (0.04)	0.29 (0.00)	4.9 (0.1)	-	-	0.054 (0.001)
LHCII mon.	0.082 (0.006)	0.26 (0.05)	0.14 (0.00)	8.3 (0.6)	-	-	0.190 (0.002)

[a]The results are rounded to 2 significant figures. The lifetimes are in picoseconds. Standard deviations are shown in brackets.

https://doi.org/10.1021/acs.jpclett.5c02240
J. Phys. Chem. Lett. XXXX, XXX, XXX−XXX

into the coarse-grained 2DES (CG-2DES) routine[46] to calculate 2D spectra and anisotropy kinetics. The calculation details are provided in the SI.

Here, we use the TD-MCFRET and CG-2DES methods for their computational efficiency in modeling large photosynthetic systems such as M-CP_2. However, the methods come with certain limitations. Since the calculations involve a high number of chromophores, their outcomes are highly sensitive to input parameters, which can significantly influence the calculated EET rates. Recognizing these limitations, we do not try to tune the calculation to match the experimental data. Instead, the results from the calculation are used as reference points to provide insights into the intersubunit dynamics of the complexes.

We first use TD-MCFRET to evaluate the effective EET times between subunits. This is done by determining the population transfer time scales between subunit pairs using the intra- and intersubunit rates from the TD-MCFRET results. More details of the estimation and the resulting effective EET times are summarized in Supporting Table S3. As these microscopic time scales are not directly observable, the characteristic EET processes of the system can be determined instead, by diagonalizing the effective EET rate (inverse lifetime) matrix from Table S3. The result shows that the overall dynamics undergoes four main processes and can be found in Figure 4. The fastest EET process occurs at 1.3 ps,

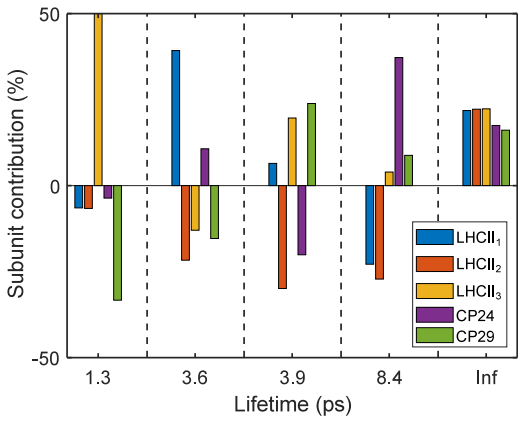

Figure 4. Characteristic EET processes in M-CP_2 obtained by diagonalizing the effective intersubunit EET rate matrix from TD-MCFRET results. Clusters of colored bars are associated with an EET time scale. Within a cluster, each colored bar corresponds to a specific subunit and the bar height gives the relative contribution of that subunit to the given time scale. Opposite-sign amplitudes can be interpreted as donor−acceptor subunits.

mostly between $LHCII_3$ and CP29. The next processes are at 3.6 and 3.9 ps, involving energy equilibration among all subunits in M-CP_2. The process at 8.4 ps occurs between $LHCII_{1-2}$ and CP24, probably with $LHCII_3$ as the intermediate. The final, nondecaying process only shows the final equilibrium population and can be neglected. In comparison, we show in Supporting Figure S5 the calculated characteristic EET processes in trimeric LHCII, where only lifetimes of 3.6−3.8 ps are present. Therefore, with CP24 and CP29 subunits included in the EET calculations, there will be additional EET processes at time scales of 1.3 and 8.4 ps.

The calculated anisotropies from CG-2DES at different excitation wavelengths (see Supporting Figure S6a) show similar behaviors as the 2DREAM results in Figure 2b. Comparing between the systems, the calculation also shows that residual anisotropy values are the highest in LHCII monomers, followed by M-CP_2 and finally LHCII trimers (Supporting Figure S6b). We consider the calculated anisotropy kinetics after T_w = 1 ps since CG-2DES presumes that excitons reach an equilibrium within their respective segments prior to detection. Analysis shows that the calculated anisotropy kinetics of the LHCII trimers can be best fitted with a single decay lifetime of 3.1 ps, while that of the M-CP_2 is best fitted with two components at 1.8 and 5.9 ps (Supporting Figures S6c-d and Table S4).

The complex calculations from TD-MCFRET and CG-2DES, to eventually obtaining the calculated anisotropy kinetics, add layers of convolutions. As a result, the calculated anisotropy decay lifetimes in M-CP_2 partially average over a weighted combination of multiple characteristic time scales of the EET processes. For example, the 1.8 ps anisotropy lifetime derives from the 1.3 and 3.6 ps characteristic EET processes in Figure 4, while the 5.9 ps lifetime derives from the 3.9 and 8.4 ps EET processes.

We can compare the calculated anisotropy kinetics components to the second and third decay components of the experimental anisotropy in Table 2 for LHCII trimer (τ_2 = 4.9 ps) and M-CP_2 (τ_2 = 3.7 ps and τ_3 = 24 ps), respectively. The calculated anisotropy kinetics in M-CP_2 is consistent with the trend in experimental data, with a slow component τ_3 for M-CP_2 that is lacking in LHCII trimers, and a fast component τ_2 that is slower for the LHCII trimers. It can be observed that the calculated time scales are, however, consistently faster than the experimental values. This can be partially attributed to the modeling and calculation procedure that causes an overestimation of the EET rates, as mentioned earlier. The choice of structures (the calculation used the protein structure derived from the supercomplex state) and parameters used, such as disorder levels and coupling strengths, can greatly affect the predicted rates. For instance, the coupling strengths inputs are based on the TrEsp method,[47−49] which can be used to reduce the EET rates with adjustments to the dielectric constant. Furthermore, the use of coarse-graining can also reduce friction from intrasegment relaxation, which leads to faster intersegment EET. Nevertheless, based on the trends, we can associate the experimental 24 ps decay to the calculated 5.9 ps decay, which originates from the 8.4 ps characteristic EET time. We can thereby make the assignment that the experimental 24 ps component has major contributions from the intersubunit EET between $LHCII_{1-2}$ and CP24.

Next, based on the assignments made above, we construct a kinetic model to phenomenologically describe the anisotropy kinetics during energy equilibration between the subunits. This model will allow us to get a "big picture" idea of the intersubunit EET. Here, each subunit in M-CP_2 is represented by a population state with the same transition dipole strength, as depicted in Figure 5a. From a top-down view, their relative rotation angles are set according to Table 1, while the angle to the plane normal axis is described by a fitting parameter θ, which will determine the residual anisotropy. We are interested in the $LHCII_{1-3}$ intersubunit EET rates (k_1) and the CP24-$LHCII_3$ rate (k_2). For the CP29-$LHCII_3$ (k_3) and CP29-CP24 (k_4) connection rates, we make use of the results from TD-MCFRET calculations (Supporting Table S3) to define fixed ratios k_2:k_3:k_4 as 1:4:0.6. The model describes the anisotropy decay kinetics through population evolution, then the

https://doi.org/10.1021/acs.jpclett.5c02240
J. Phys. Chem. Lett. XXXX, XXX, XXX−XXX

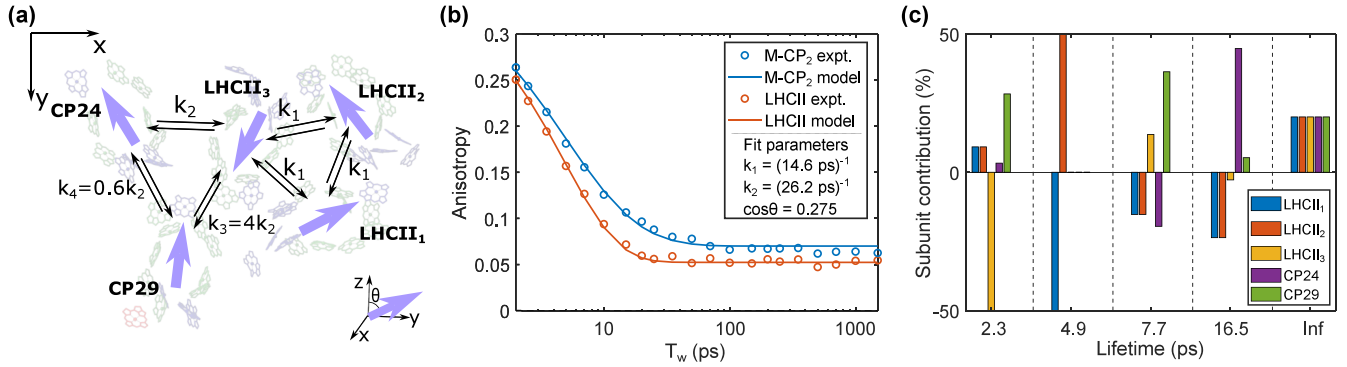

Figure 5. Phenomenological kinetic model describing the intersubunit EET processes in M-CP_2 that cause the anisotropy decay. (a) Illustration of the modeled EET connections between the M-CP_2 subunits. The subunits are aligned in the same xy-plane. In addition, all transition dipoles form the same polar angle θ with the plane normal (z-axis). (b) The fitted anisotropy decays (solid curves) compared with the experimental data (circles). The fitted parameters are also indicated. (c) Characteristic EET processes obtained by diagonalizing the EET rate matrix from the kinetic model. The presentation is the same as in Figure 4.

simulated decay curve is fitted to the 2DREAM data in Figure 3 to find the suitable intersubunit EET rates. More details about the model can be found in the SI.

This phenomenological kinetic model is capable of reproducing the anisotropy dynamics in LHCII trimers and M-CP_2, as the modeled anisotropies show almost identical decay trends to the experimental data (Figure 5b). The fitted EET rates between the three monomers of LHCII (k_1) are found to be $(14.6\ \text{ps})^{-1}$. This fits well with the 4.9 ps anisotropy decay component observed in LHCII trimers (Table 2), which is three-time faster than the monomer−monomer EET due to the 3-fold symmetry of the complex.[50] The connection from CP24 to $LHCII_3$ is found to be $k_2 = (26.2\ \text{ps})^{-1}$. Correspondingly, the CP29-$LHCII_3$ EET rate is $k_3 = 4k_2 = (6.6\ \text{ps})^{-1}$ and the CP24-CP29 rate is $k_4 = 0.6k_2 = (43.6\ \text{ps})^{-1}$. Furthermore, the cosine of the polar angle θ is fitted to be 0.275. This corresponds to an approximate angle of 16° from the representative transition dipole of the lowest energy states to the complex plane. Such value is close to results from polarized absorption and fluorescence measurements of macroscopically aligned LHCII trimers, where the authors found an angle of 17.5° ± 2.5°.[51] It is worth noting that this angle is also applicable to the M-CP_2 complex, implying that CP24 and CP29 are similar to LHCII monomers regarding the composition of the Chl molecules composing the terminal energy states.

We compare the fitted EET times from the kinetic model in Figure 5 to the results from TD-MCFRET calculation in Supporting Table S3. The EET times between the LHCII monomeric units see a good agreement between the two approaches, where the figure from the kinetic model (14.6 ps) matches relatively well with 11−12 ps from TD-MCFRET, considering the overestimation from coarse-graining. However, in the EET between LHCII and the CPs, there appears a large contrast between the methods. The ratio between the LHCII−LHCII and LHCII-CP24 rates, k_1:k_2, is found to be almost 2 in the kinetic model. Meanwhile, this ratio from TD-MCFRET results is much lower, at around 1.2 (ratio between 14 and 12 ps). Hence, it suggests that the interaction strengths between LHCII(M), CP29, and CP24, are almost twice as weak as the expected strengths estimated from the structure-based energy transfer theory.

Analogous to the TD-MCFRET analysis in Figure 4, we have the characteristic EET times from the phenomenological kinetic model (see Figure 5c). The fast component of 2.3 ps is analogous to the calculated 1.3 ps component in Figure 4. This component likewise enhances the energy equilibration in the LHCII(M)-CP29 cluster and together with the 4.9 ps component results in the accelerated 3.7 ps anisotropy process measured in M-CP_2. Without this, the measurable anisotropy time scale is 4.9 ps, as measured in the LHCII trimer. CP29 and LHCII(M) are well connected, and is in line with the interpretation that CP29 is a connecting bridge and a possible nonphotochemical quenching site for energy flowing between LHCII(M) and the PSII core complex.[24,52−54] The slowest EET component from the phenomenological kinetic model is 16.5 ps. This time scale is twice as long as the slowest lifetime (8.4 ps) obtained from TD-MCFRET and relatively more distinguishable from the intermediate processes (4.9−7.7 ps, Figure 5c). The kinetic model thus captures the slower anisotropy dynamics in the experimental data more accurately and further supports that the long-lived (24 ps) anisotropy decay is a population equilibration process between LHCII(M) and the CP24 subunit. We note that the 16.5 ps lifetime is still faster than the experimental 24 ps component, which is due to the constraints in the model, such as the fixed ratios between the EET rates.

We discuss the assignment of the sub-ps EET processes as observed in Table 2. As a rule of thumb, EET processes happening within a monomeric subunit (intrasubunit) generally occur faster than those involving intersubunit connections. We consider the first anisotropy decay component in Table 2. Despite the different antenna sizes, the amplitudes and lifetimes of this component appear to be similar between the three studied complexes. The averaged amplitude is 0.06 and the averaged lifetime is 0.25 ps. This decay component only causes a small drop in anisotropy value (out of 0.4), suggesting that the underlying EET processes occur between similarly oriented molecules. Sub-ps EET processes in LHCII has been assigned to Chl b-to-a energy transfer and energy equilibration within some Chl a domains in LHCII, which mostly occur within a monomeric subunit.[7,9,10,55] Thus, the sub-ps depolarization process likely corresponds to the first intrasubunit EET steps from the initial excited Chl molecules to their nearest neighbors, which are also strongly coupled to each other with their similar transition dipole orientations.

https://doi.org/10.1021/acs.jpclett.5c02240
J. Phys. Chem. Lett. XXXX, XXX, XXX−XXX

For the second anisotropy decay component, although there is no consensus on the contributions from intra- and intersubunit processes, many insights can be obtained by comparing between LHCII trimers and monomers. The lifetime of this component in monomeric LHCII is 8.3 ps, and in the trimeric complex is 4.9 ps. Different explanations can be provided. In monomeric LHCII, energy equilibration among weakly connected Chl *a* domains likely causes the 8.3 ps anisotropy decay. Trimerization produces faster decay due to additional EET pathways linking domains across subunits. Most intermonomeric transfer occurs between Chl *a*602−*a*603 domains,[9,10] but other routes, such as from Chl *a*613−*a*614 to *a*602−*a*603 in neighboring monomers, show similar coupling strengths.[9] These pathways promote rapid equilibration throughout the trimer, reducing the impact of slower monomeric processes. Another explanation for the slower anisotropy decay in LHCII monomers can be attributed to possible changes in the protein conformation of LHCII after the monomerization procedure. Compared to the trimeric form, the monomeric LHCII is more exposed to the solvent. This possibly leads to changes to the chromophore local environments, affecting their site energies and coupling strengths, and perhaps even a loss of chromophores.[56,57] As these structural changes are not included in the structure-based TD-MCFRET and CG-2DES calculations, this may also explain why the calculated anisotropy decay in monomeric LHCII is not so different from the trimeric counterpart.

Taking the explanations together, the agreement is that the 8.3 ps decay process in monomeric LHCII is not relevant in the aggregated state, so we will not consider this lifetime in the dynamics of the larger complexes. In analyzing the TD-MCFRET results and the phenomenological kinetic model, we adopt a simplified representation of EET between subunits that appears to omit intrasubunit processes. However, the EET times in these models effectively reflect the combined influence of all (both intra- and intersubunit) transfer pathways and thus implicitly account for intrasubunit EET contributions. Moreover, in the case that some slow intrasubunit EET processes may affect the overall intersubunit population flow, their interplay can be effectively incorporated and described as an equivalent intersubunit process as shown in Supporting Figure S8.

Regarding the differences in interaction strengths obtained from the structure-based TD-MCFRET and phenomenological simulations, it may reflect the structural difference of the M-CP_2 complex between the solubilized and supercomplex state. Comparing the results from the two methods, we suggest that CP24, CP29, and LHCII(M) in the solubilized M-CP_2 samples could be slightly displaced from each other and this results in at least 2-fold decrease in the EET rates between them. Assuming that the energy transfer rate scales inversely with the sixth power of donor−acceptor distance, a 2-fold decrease in EET rate should correspond to a 12% increase in intersubunit distances. This shows the high sensitivity of intersubunit EET to their relative distances. At physiological condition, such fluctuations in intersubunit organization are highly possible. In fact, structural studies of PSII reported substantial flexibility and displacements of the proteins in the supercomplex.[58,59] Furthermore, while the cryo-EM or crystal structures are often relied as a basis for calculating spectral features and energy transfer dynamics, they are static and do not capture the dynamic conformational flexibility of the proteins at physiological temperatures. It has been highlighted that protein structures can influence spectral and EET properties and simulations of their dynamics is necessary.[18,60,61] Therefore, though they may not be reflected in the cryo-EM structure, slow EET connections, such as the 24 ps component that we observed, are still likely to be relevant as a result of the influence of thermal fluctuation effects to the protein structures. The degree of influence of such effects is nontrivial and requires further studies, preferably with the help of molecular dynamics simulations.

We have demonstrated that 2DREAM could provide detailed insights to the intersubunit EET processes, by utilizing the relative exciton orientations between the energy states. Derived from simultaneously collected polarized 2DES signals, 2DREAM assumes good consistency in experimental conditions, high anisotropy data quality, and the time and frequency resolution inherent in 2DES. Measuring the anisotropy also has the advantage that the lifetimes appearing on the anisotropy decay kinetics should theoretically reflect the most prominent time scales of the energy equilibration process. Apart from being the benchmarks for intersubunit EET processes at room temperature, our present results will also open up the possibility of monitoring the EET dynamics in larger systems, such as the PSII supercomplex and even the photosystems *in vivo*. However, it is not without limitations: anisotropy kinetics do not reflect EET processes that involve small changes in exciton orientations. This can cause the anisotropy decay to miss out certain EET processes, especially systems with similarly oriented chromophores, or in large multichromophoric systems where the anisotropic distribution can be washed out after a certain number of diffusion steps.

It is worth mentioning that exciton−exciton annihilation (EEA) time may also be used as a measure for the equilibration process in large multichromophoric systems.[62] Studies measuring EEA in LHCII trimers and LHCII aggregates found annihilation times of around 25 ps in LHCII trimers and 40 ps in M-CP_2.[21,63−65] It has been argued that the spatial equilibration rate can be estimated to be half of the annihilation rate, due to the latter involving movements of two excitons.[64,66] Assuming that spatial and energy equilibrations are similar, this leads to energy equilibration times in LHCII trimers and M-CP_2 being 50 and 80 ps, respectively, based on their EEA time scales. These times appeared to be significantly slower than the anisotropy decay time scales measured in our work here. There are however indications that the relation between the measured EEA and actual equilibration rates are more complex.[67,68] It was suggested that factors such as sample size constraints, presence of traps, and the excitation beam profile could influence the interpretation of annihilation kinetics.[68,69] Hence, the energy equilibration time may not be reliably inferred from the annihilation decay time, and a direct comparison between our results and the EEA times is not trivial. We suggest that a combination of several methods, including anisotropy, EEA, and isotropic population dynamics, is still needed to accurately determine the energy equilibration time in multichromophoric systems.

In conclusion, we performed a time-resolved anisotropy study based on the polarization-resolved 2DES to resolve the EET processes between the antenna LHCs in PSII. The spectral overlap between subunits, rather than being a disadvantage, is instead utilized to highlight orientational dynamics between the isoenergetic states. This allows us to observe intersubunit EET processes between the LHCs in

https://doi.org/10.1021/acs.jpclett.5c02240
J. Phys. Chem. Lett. XXXX, XXX, XXX−XXX

physiological conditions, whereas it often requires cryogenic temperatures to be able to discern the spectral kinetics of such processes. The measurements on M-CP_2, LHCII trimers, and LHCII monomers are compared to each other and reveal multiple anisotropy decay lifetimes corresponding to different intra- and intersubunit EET processes. With the help of theoretical calculations and phenomenological kinetic modeling, the EET rates between the subunits can also be estimated to understand the anisotropy decay kinetics. The sub-ps anisotropy decays can be assigned with intrasubunit origins due to their similar appearances in the three complexes. Meanwhile, the several-ps anisotropy decay is accelerated in M-CP_2 compared to LHCII trimers, which suggests fast energy equilibration processes in the larger complexes facilitated by intersubunit EET. We observe that the several-ps decay process in the M-CP_2 complex is accelerated, while a long-lived process also presents, which can be attributed to the intersubunit energy equilibration between LHCII(M) trimer and the minor antenna CP24.

Our results imply that the connectivity between the M-CP_2 subunits can vary between each specific pair, which can be attributed to the sensitivity of intersubunit EET to the interprotein arrangement. These findings can serve as a basis to evaluate the overall light energy dynamics within photosystems and the specific roles played by individual components. The high sensitivity of the EET rates to the protein arrangement suggests large variations in the overall EET dynamics of the PSII with disturbances from structural fluctuations. It is probable that the relatively "flat" energy landscape in PSII could allow the LHC subunits to participate in the EET network and maintain the overall connectivity even in the presence of structural variations. This ensures multiple EET pathways for an excitation to reach the RC even when some of the intersubunit EET connections are weakened. While such design can limit the maximum efficiency of the EET processes, it ensures the EET flow to be flexible and a general robustness to the system.

■ ASSOCIATED CONTENT

Data Availability Statement

Data for this article, including linear absorption, pump spectrum, and 2DES spectra, are available at https://zenodo.org/records/15551331.

Supporting Information

The Supporting Information is available free of charge at https://pubs.acs.org/doi/10.1021/acs.jpclett.5c02240.

Experimental methods, additional experimental data, details about reconstructing 2DES signals at different polarizations, choosing the exponential fit, lifetime distribution analysis, TD-MCFRET calculation details, phenomenological kinetic model details, and the modeling of anisotropy decays in LHCII monomers and trimers (PDF)

Transparent Peer Review report available (PDF)

■ AUTHOR INFORMATION

Corresponding Author

Howe-Siang Tan − *School of Chemistry, Chemical Engineering and Biotechnology, Nanyang Technological University, 637371, Singapore;* orcid.org/0000-0003-2523-106X; Email: howesiang@ntu.edu.sg

Authors

Hoang Long Nguyen − *School of Chemistry, Chemical Engineering and Biotechnology, Nanyang Technological University, 637371, Singapore*

Kai Zhong − *Zernike Institute for Advanced Materials, University of Groningen, 9747 AG Groningen, The Netherlands; School of Chemistry, Chemical Engineering and Biotechnology, Nanyang Technological University, 637371, Singapore;* orcid.org/0000-0001-5441-3079

Thanh Nhut Do − *Department of Physics and Astronomy, Faculty of Science, Vrije Universiteit Amsterdam, 1081 HZ Amsterdam, The Netherlands;* orcid.org/0000-0002-5155-6936

Parveen Akhtar − *HUN-REN Biological Research Centre Szeged, Szeged 6726, Hungary;* orcid.org/0000-0002-3264-7154

Petar H. Lambrev − *HUN-REN Biological Research Centre Szeged, Szeged 6726, Hungary;* orcid.org/0000-0001-5147-153X

Thomas L. C. Jansen − *Zernike Institute for Advanced Materials, University of Groningen, 9747 AG Groningen, The Netherlands;* orcid.org/0000-0001-6066-6080

Jasper Knoester − *Zernike Institute for Advanced Materials, University of Groningen, 9747 AG Groningen, The Netherlands; Faculty of Science, Leiden University, 2300 RA Leiden, The Netherlands*

Stefano Caffarri − *Aix Marseille Université, CEA, CNRS, BIAM, LGBP, 13009 Marseille, France*

Complete contact information is available at: https://pubs.acs.org/10.1021/acs.jpclett.5c02240

Notes

The authors declare no competing financial interest.

■ ACKNOWLEDGMENTS

This work was supported by Singapore Ministry of Education Academic Research Fund, MOE-T2EP50122-0022 and RG92/23 (H.-S.T.); National Research, Development and Innovation Fund, FK-139067 (P.A.) and ANN-144012 (P.L.); and The Hungarian Research Network, KMP-2024-23 (P.A.). We thank the Center for Information Technology of the University of Groningen for their support and for providing access to the Hábrók high performance computing cluster.

■ REFERENCES

(1) Blankenship, R. *Molecular Mechanisms of Photosynthesis*; Wiley, 2014.

(2) Caffarri, S.; Kouřil, R.; Kereïche, S.; Boekema, E. J.; Croce, R. Functional Architecture of Higher Plant Photosystem II Supercomplexes. *EMBO J.* **2009**, *28*, 3052−3063.

(3) Cao, P.; Su, X.; Pan, X.; Liu, Z.; Chang, W.; Li, M. Structure, Assembly and Energy Transfer of Plant Photosystem II Supercomplex. *Biochim. Biophys. Acta BBA - Bioenerg.* **2018**, *1859*, 633−644.

(4) van Grondelle, R.; Novoderezhkin, V. I. Energy Transfer in Photosynthesis: Experimental Insights and Quantitative Models. *Phys. Chem. Chem. Phys.* **2006**, *8*, 793−807.

(5) de Bianchi, S.; Dall'Osto, L.; Tognon, G.; Morosinotto, T.; Bassi, R. Minor Antenna Proteins CP24 and CP26 Affect the Interactions between Photosystem II Subunits and the Electron Transport Rate in Grana Membranes of Arabidopsis. *Plant Cell* **2008**, *20*, 1012−28.

(6) Marin, A.; Passarini, F.; Croce, R.; van Grondelle, R. Energy Transfer Pathways in the CP24 and CP26 Antenna Complexes of

Higher Plant Photosystem II: A Comparative Study. *Biophys. J.* **2010**, *99*, 4056−4065.
(7) Schlau-Cohen, G. S.; Calhoun, T. R.; Ginsberg, N. S.; Read, E. L.; Ballottari, M.; Bassi, R.; van Grondelle, R.; Fleming, G. R. Pathways of Energy Flow in LHCII from Two-Dimensional Electronic Spectroscopy. *J. Phys. Chem. B* **2009**, *113*, 15352−15363.
(8) Croce, R.; van Amerongen, H. Light-Harvesting and Structural Organization of Photosystem II: From Individual Complexes to Thylakoid Membrane. *J. Photochem. Photobiol., B* **2011**, *104*, 142−153.
(9) Novoderezhkin, V.; Marin, A.; van Grondelle, R. Intra- and Inter-Monomeric Transfers in the Light Harvesting LHCII Complex: The Redfield-Forster Picture. *Phys. Chem. Chem. Phys.* **2011**, *13*, 17093−103.
(10) Renger, T.; Madjet, M. E.; Knorr, A.; Müh, F. How the Molecular Structure Determines the Flow of Excitation Energy in Plant Light-Harvesting Complex II. *J. Plant Physiol.* **2011**, *168*, 1497−509.
(11) Duan, H.-G.; Stevens, A. L.; Nalbach, P.; Thorwart, M.; Prokhorenko, V. I.; Miller, R. J. D. Two-Dimensional Electronic Spectroscopy of Light-Harvesting Complex II at Ambient Temperature: A Joint Experimental and Theoretical Study. *J. Phys. Chem. B* **2015**, *119*, 12017−12027.
(12) Akhtar, P.; Zhang, C.; Do, T. N.; Garab, G.; Lambrev, P. H.; Tan, H.-S. Two-Dimensional Spectroscopy of Chlorophyll a Excited-State Equilibration in Light-Harvesting Complex II. *J. Phys. Chem. Lett.* **2017**, *8*, 257−263.
(13) Pan, J.; Gelzinis, A.; Chorošajev, V.; Vengris, M.; Senlik, S. S.; Shen, J.-R.; Valkunas, L.; Abramavicius, D.; Ogilvie, J. P. Ultrafast Energy Transfer within the Photosystem II Core Complex. *Phys. Chem. Chem. Phys.* **2017**, *19*, 15356−15367.
(14) Do, T. N.; Huerta-Viga, A.; Akhtar, P.; Nguyen, H. L.; Nowakowski, P. J.; Khyasudeen, M. F.; Lambrev, P. H.; Tan, H.-S. Revealing the Excitation Energy Transfer Network of Light-Harvesting Complex II by a Phenomenological Analysis of Two-Dimensional Electronic Spectra at 77 K. *J. Chem. Phys.* **2019**, *151*, 205101.
(15) Broess, K.; Trinkunas, G.; van Hoek, A.; Croce, R.; van Amerongen, H. Determination of the Excitation Migration Time in Photosystem II. *Biochim. Biophys. Acta BBA - Bioenerg.* **2008**, *1777*, 404−409.
(16) Bennett, D. I. G.; Fleming, G. R.; Amarnath, K. Energy-Dependent Quenching Adjusts the Excitation Diffusion Length to Regulate Photosynthetic Light Harvesting. *Proc. Natl. Acad. Sci. U. S. A.* **2018**, *115*, E9523−E9531.
(17) Caffarri, S.; Broess, K.; Croce, R.; van Amerongen, H. Excitation Energy Transfer and Trapping in Higher Plant Photosystem II Complexes with Different Antenna Sizes. *Biophys. J.* **2011**, *100*, 2094−2103.
(18) Do, T. N.; Nguyen, H. L.; Akhtar, P.; Zhong, K.; Jansen, T. L. C.; Knoester, J.; Caffarri, S.; Lambrev, P. H.; Tan, H.-S. Ultrafast Excitation Energy Transfer Dynamics in the LHCII−CP29−CP24 Subdomain of Plant Photosystem II. *J. Phys. Chem. Lett.* **2022**, *13*, 4263−4271.
(19) Nguyen, H. L.; Do, T. N.; Zhong, K.; Akhtar, P.; Jansen, T. L. C.; Knoester, J.; Caffarri, S.; Lambrev, P.; Tan, H.-S. Inter-Subunit Energy Transfer Processes in a Minimal Plant Photosystem II Supercomplex. *Sci. Adv.* **2024**, *10*, No. eadh0911.
(20) Leonardo, C.; Yang, S.-J.; Orcutt, K.; Iwai, M.; Arsenault, E. A.; Fleming, G. R. Bidirectional Energy Flow in the Photosystem II Supercomplex. *J. Phys. Chem. B* **2024**, *128*, 7941−7953.
(21) Elias, E.; Hu, C.; Croce, R. Inter-Protein Energy Transfer Dynamics in the PSII Antenna. *Cell Rep. Phys. Sci.* **2024**, *5*, 102198.
(22) Croce, R.; van Amerongen, H. Natural Strategies for Photosynthetic Light Harvesting. *Nat. Chem. Biol.* **2014**, *10*, 492−501.
(23) Kreisbeck, C.; Aspuru-Guzik, A. Efficiency of Energy Funneling in the Photosystem II Supercomplex of Higher Plants. *Chem. Sci.* **2016**, *7*, 4174−4183.
(24) Yang, S.-J.; Wales, D. J.; Woods, E. J.; Fleming, G. R. Design Principles for Energy Transfer in the Photosystem II Supercomplex from Kinetic Transition Networks. *Nat. Commun.* **2024**, *15*, 8763.
(25) Hamm, P.; Zanni, M. *Concepts and Methods of 2D Infrared Spectroscopy*; Cambridge University Press: Cambridge, 2011.
(26) Mukamel, S. *Principles of Nonlinear Optical Spectroscopy*; Oxford University Press: New York, 1995.
(27) Hochstrasser, R. M. Two-Dimensional IR-spectroscopy: Polarization Anisotropy Effects. *Chem. Phys.* **2001**, *266*, 273−284.
(28) Song, Y.; Schubert, A.; Maret, E.; Burdick, R. K.; Dunietz, B. D.; Geva, E.; Ogilvie, J. P. Vibronic Structure of Photosynthetic Pigments Probed by Polarized Two-Dimensional Electronic Spectroscopy and Ab Initio Calculations. *Chem. Sci.* **2019**, *10*, 8143−8153.
(29) Ginsberg, N. S.; Davis, J. A.; Ballottari, M.; Cheng, Y.-C.; Bassi, R.; Fleming, G. R. Solving Structure in the CP29 Light Harvesting Complex with Polarization-Phased 2D Electronic Spectroscopy. *Proc. Natl. Acad. Sci. U. S. A.* **2011**, *108*, 3848−3853.
(30) Schlau-Cohen, G. S.; Calhoun, T. R.; Ginsberg, N. S.; Ballottari, M.; Bassi, R.; Fleming, G. R. Spectroscopic Elucidation of Uncoupled Transition Energies in the Major Photosynthetic Light-Harvesting Complex, LHCII. *Proc. Natl. Acad. Sci. U. S. A.* **2010**, *107*, 13276−13281.
(31) Xiong, W.; Zanni, M. T. Signal Enhancement and Background Cancellation in Collinear Two-Dimensional Spectroscopies. *Opt. Lett.* **2008**, *33*, 1371−1373.
(32) Read, E. L.; Engel, G. S.; Calhoun, T. R.; Mančal, T.; Ahn, T. K.; Blankenship, R. E.; Fleming, G. R. Cross-Peak-Specific Two-Dimensional Electronic Spectroscopy. *Proc. Natl. Acad. Sci. U. S. A.* **2007**, *104*, 14203−14208.
(33) Voronine, D. V.; Abramavicius, D.; Mukamel, S. Manipulating Multidimensional Electronic Spectra of Excitons by Polarization Pulse Shaping. *J. Chem. Phys.* **2007**, *126*, 044508.
(34) Bukartė, E.; Haufe, A.; Paleček, D.; Büchel, C.; Zigmantas, D. Revealing Vibronic Coupling in Chlorophyll C1 by Polarization-Controlled 2D Electronic Spectroscopy. *Chem. Phys.* **2020**, *530*, 110643.
(35) Leng, X.; Yan, Y.; Zhu, R.; Zou, J.; Zhang, W.; Shi, Q. Revealing Intermolecular Electronic and Vibronic Coherence with Polarization-Dependent Two-Dimensional Beating Maps. *J. Phys. Chem. Lett.* **2023**, *14*, 838−845.
(36) Massey, S. C.; Ting, P.-C.; Yeh, S.-H.; Dahlberg, P. D.; Sohail, S. H.; Allodi, M. A.; Martin, E. C.; Kais, S.; Hunter, C. N.; Engel, G. S. Orientational Dynamics of Transition Dipoles and Exciton Relaxation in LH2 from Ultrafast Two-Dimensional Anisotropy. *J. Phys. Chem. Lett.* **2019**, *10*, 270−277.
(37) Marin, A.; van Stokkum, I. H. M.; Novoderezhkin, V. I.; van Grondelle, R. Excitation-Induced Polarization Decay in the Plant Light-Harvesting Complex LHCII. *J. Photochem. Photobiol. Chem.* **2012**, *234*, 91−99.
(38) Kwa, S. L. S.; van Amerongen, H.; Lin, S.; Dekker, J. P.; van Grondelle, R.; Struve, W. S. Ultrafast Energy Transfer in LHC-II Trimers from the Chl *a*/*b* Light-Harvesting Antenna of Photosystem II. *Biochim. Biophys. Acta BBA - Bioenerg.* **1992**, *1102*, 202−212.
(39) Du, M.; Xie, X.; Mets, L.; Fleming, G. R. Direct Observation of Ultrafast Energy-Transfer Processes in Light Harvesting Complex II. *J. Phys. Chem.* **1994**, *98*, 4736−4741.
(40) Savikhin, S.; van Amerongen, H.; Kwa, S. L.; van Grondelle, R.; Struve, W. S. Low-Temperature Energy Transfer in LHC-II Trimers from the Chl a/b Light-Harvesting Antenna of Photosystem II. *Biophys. J.* **1994**, *66*, 1597−1603.
(41) Su, X.; Ma, J.; Wei, X.; Cao, P.; Zhu, D.; Chang, W.; Liu, Z.; Zhang, X.; Li, M. Structure and Assembly Mechanism of Plant C2S2M2-type PSII-LHCII Supercomplex. *Science* **2017**, *357*, 815−820.
(42) Xu, P.; Roy, L. M.; Croce, R. Functional Organization of Photosystem II Antenna Complexes: CP29 under the Spotlight. *Biochim. Biophys. Acta BBA - Bioenerg.* **2017**, *1858*, 815−822.
(43) Jonas, D. M.; Lang, M. J.; Nagasawa, Y.; Joo, T.; Fleming, G. R. Pump-Probe Polarization Anisotropy Study of Femtosecond Energy

https://doi.org/10.1021/acs.jpclett.5c02240
J. Phys. Chem. Lett. XXXX, XXX, XXX−XXX

Transfer within the Photosynthetic Reaction Center of Rhodobacter Sphaeroides R26. *J. Phys. Chem.* **1996**, *100*, 12660−12673.
(44) Shiu, Y. J.; Shi, Y.; Hayashi, M.; Su, C.; Han, K. L.; Lin, S. H. Femtosecond Spectroscopy Study of Electronically Excited States of *Chlorophyll a* Molecules in Ethanol. *Chem. Phys. Lett.* **2003**, *378*, 202−210.
(45) Zhong, K.; Nguyen, H. L.; Do, T. N.; Tan, H.-S.; Knoester, J.; Jansen, T. L. C. An Efficient Time-Domain Implementation of the Multichromophoric Förster Resonant Energy Transfer Method. *J. Chem. Phys.* **2023**, *158*, 064103.
(46) Zhong, K.; Nguyen, H. L.; Do, T. N.; Tan, H.-S.; Knoester, J.; Jansen, T. L. C. Coarse-Grained Approach to Simulate Signatures of Excitation Energy Transfer in Two-Dimensional Electronic Spectroscopy of Large Molecular Systems. *J. Chem. Theory Comput.* **2024**, *20*, 6111−6124.
(47) Madjet, M. E.; Abdurahman, A.; Renger, T. Intermolecular Coulomb Couplings from Ab Initio Electrostatic Potentials: Application to Optical Transitions of Strongly Coupled Pigments in Photosynthetic Antennae and Reaction Centers. *J. Phys. Chem. B* **2006**, *110*, 17268−17281.
(48) Renger, T. Theory of Excitation Energy Transfer: From Structure to Function. *Photosynth. Res.* **2009**, *102*, 471−85.
(49) van der Vegte, C. P.; Prajapati, J. D.; Kleinekathöfer, U.; Knoester, J.; Jansen, T. L. C. Atomistic Modeling of Two-Dimensional Electronic Spectra and Excited-State Dynamics for a Light Harvesting 2 Complex. *J. Phys. Chem. B* **2015**, *119*, 1302−1313.
(50) Lyle, P. A.; Struve, W. S. Dynamic Linear Dichroism in Chromoproteins. *Photochem. Photobiol.* **1991**, *53*, 359−365.
(51) van Amerongen, H.; Kwa, S. L.; van Bolhuis, B. M.; van Grondelle, R. Polarized Fluorescence and Absorption of Macroscopically Aligned Light Harvesting Complex II. *Biophys. J.* **1994**, *67*, 837−847.
(52) Miloslavina, Y.; de Bianchi, S.; Dall'Osto, L.; Bassi, R.; Holzwarth, A. R. Quenching in *Arabidopsis Thaliana* Mutants Lacking Monomeric Antenna Proteins of Photosystem II. *J. Biol. Chem.* **2011**, *286*, 36830−36840.
(53) Fox, K. F.; Ünlü, C.; Balevičius, V.; Ramdour, B. N.; Kern, C.; Pan, X.; Li, M.; van Amerongen, H.; Duffy, C. D. P. A Possible Molecular Basis for Photoprotection in the Minor Antenna Proteins of Plants. *Biochim. Biophys. Acta BBA - Bioenerg.* **2018**, *1859*, 471−481.
(54) Mascoli, V.; Novoderezhkin, V.; Liguori, N.; Xu, P.; Croce, R. Design Principles of Solar Light Harvesting in Plants: Functional Architecture of the Monomeric Antenna CP29. *Biochim. Biophys. Acta BBA - Bioenerg.* **2020**, *1861*, 148156.
(55) Akhtar, P.; Do, T. N.; Nowakowski, P. J.; Huerta-Viga, A.; Khyasudeen, M. F.; Lambrev, P. H.; Tan, H.-S. Temperature Dependence of the Energy Transfer in LHCII Studied by Two-Dimensional Electronic Spectroscopy. *J. Phys. Chem. B* **2019**, *123*, 6765−6775.
(56) Kleima, F. J.; Gradinaru, C. C.; Calkoen, F.; van Stokkum, I. H. M.; van Grondelle, R.; van Amerongen, H. Energy Transfer in LHCII Monomers at 77K Studied by Sub-Picosecond Transient Absorption Spectroscopy. *Biochemistry* **1997**, *36*, 15262−15268.
(57) Gradinaru, C. C.; Özdemir, S.; Gülen, D.; van Stokkum, I. H. M.; van Grondelle, R.; van Amerongen, H. The Flow of Excitation Energy in LHCII Monomers: Implications for the Structural Model of the Major Plant Antenna. *Biophys. J.* **1998**, *75*, 3064−3077.
(58) Caspy, I.; Fadeeva, M.; Mazor, Y.; Nelson, N. Structure of Dunaliella Photosystem II Reveals Conformational Flexibility of Stacked and Unstacked Supercomplexes. *eLife* **2023**, *12*, No. e81150.
(59) Graça, A. T.; Hall, M.; Persson, K.; Schröder, W. P. High-Resolution Model of Arabidopsis Photosystem II Reveals the Structural Consequences of Digitonin-Extraction. *Sci. Rep.* **2021**, *11*, 15534.
(60) Vasil'ev, S.; Bruce, D. A Protein Dynamics Study of Photosystem II: The Effects of Protein Conformation on Reaction Center Function. *Biophys. J.* **2006**, *90*, 3062−3073.
(61) Liguori, N.; Croce, R.; Marrink, S. J.; Thallmair, S. Molecular Dynamics Simulations in Photosynthesis. *Photosynth. Res.* **2020**, *144*, 273−295.
(62) Valkunas, L.; Cervinskas, V.; van Mourik, F. Energy Transfer and Connectivity in Chloroplasts: Competition between Trapping and Annihilation in Pulsed Fluorescence Induction Experiments. *J. Phys. Chem. B* **1997**, *101*, 7327−7331.
(63) Bittner, T.; Irrgang, K.-D.; Renger, G.; Wasielewski, M. R. Ultrafast Excitation Energy Transfer and Exciton-Exciton Annihilation Processes in Isolated Light Harvesting Complexes of Photosystem II (LHC II) from Spinach. *J. Phys. Chem.* **1994**, *98*, 11821−11826.
(64) Barzda, V.; Gulbinas, V.; Kananavicius, R.; Cervinskas, V.; van Amerongen, H.; van Grondelle, R.; Valkunas, L. Singlet−Singlet Annihilation Kinetics in Aggregates and Trimers of LHCII. *Biophys. J.* **2001**, *80*, 2409−2421.
(65) Malý, P.; Lüttig, J.; Rose, P. A.; Turkin, A.; Lambert, C.; Krich, J. J.; Brixner, T. Separating Single- from Multi-Particle Dynamics in Nonlinear Spectroscopy. *Nature* **2023**, *616*, 280−287.
(66) van Amerongen, H.; van Grondelle, R. Understanding the Energy Transfer Function of LHCII, the Major Light-Harvesting Complex of Green Plants. *J. Phys. Chem. B* **2001**, *105*, 604−617.
(67) Trinkunas, G.; Herek, J. L.; Polívka, T.; Sundström, V.; Pullerits, T. Exciton Delocalization Probed by Excitation Annihilation in the Light-Harvesting Antenna LH2. *Phys. Rev. Lett.* **2001**, *86*, 4167−4170.
(68) Zhang, K.; Lee, T.-Y.; Yang, S.-J.; Bhagde, T.; Iwai, M.; Fleming, G. R. Probing Exciton Diffusion Dynamics in Photosynthetic Supercomplexes via Exciton−Exciton Annihilation. *J. Chem. Phys.* **2025**, *162*, 164201.
(69) Gharbi, A. M.; Biswas, D. S.; Crégut, O.; Malý, P.; Didier, P.; Klymchenko, A.; Léonard, J. Exciton Annihilation and Diffusion Length in Disordered Multichromophoric Nanoparticles. *Nanoscale* **2024**, *16*, 11550−11563.

https://doi.org/10.1021/acs.jpclett.5c02240
J. Phys. Chem. Lett. XXXX, XXX, XXX−XXX